PHILIPPINE ENGINEERING JOURNAL
PEJ 2022; Vol. 43, No. 1: 111-136

Received: 03 February 2022
Accepted: 15 June 2022

Estimation of Net Absolute Sea Level Change in Mogpog, Marinduque using Persistent Scatterer Interferometric Synthetic Aperture Radar-derived Vertical Land Motion and Tide Gauge Measurements

Pocholo Miguel A. De Lara, Trisha Marie D. Morado, and Rosalie B. Reyes
Department of Geodetic Engineering, College of Engineering,
University of the Philippines Diliman
Quezon City, Philippines

Abstract — *Sea level change can bring about various coastal hazards. For this reason, studies on sea level change are important in planning for the mitigation of risks caused by the said phenomenon. This research estimates the relative and net absolute sea level change in Mogpog, Marinduque using tide gauge (TG) measurements, Global Navigation Satellite System (GNSS) observations, and Persistent Scatterer Interferometric Synthetic Aperture Radar (PSInSAR) technique. Also, the vertical land motion (VLM) was investigated to determine if sea level measurements are contaminated by it. Sentinel-1 radar images in ascending and descending geometries were processed to determine the coherence, and line-of-sight (LOS) displacements and velocities of the persistent scatterer (PS) points. The PSInSAR results were validated using LOS converted GNSS data at the nearest Active Geodetic Network (AGN) station. The correlation obtained between PSInSAR and GNSS data were 0.761 and 0.796 for ascending and descending, respectively. Due to this high correlation, the PSInSAR derived VLM near the tide gauge was used in the absence of a collocated GNSS receiver at the tide gauge. The net absolute sea level change was computed by adding the contribution of VLM. The VLM rate near the Balanacan tide gauge station from PSInSAR was -3.822 ± 0.713 mm/yr. The relative sea level rate extracted from the tide gauge readings from 2007 to 2020 was 0.23 ± 0.63 mm/yr. Assuming a linear rate resulting from both datasets, the net absolute sea level change was estimated at -3.592 ± 0.951 mm/yr. The negative net absolute sea level trend was due to the strong influence of El Nino during this short period of observation. The result showed how VLM masked the actual sea level trend during the period of observation.*

Keywords — GNSS, Net Absolute Sea Level Change, PSInSAR, Relative Sea Level Change, VLM

I. INTRODUCTION

Sea level change refers to the changes in mean sea level over time due to global or local phenomena like climate change and local tectonic activities. [1]. One way to measure sea level change is by using tide gauge measurements recorded by tide gauges with respect to the local land where it is stationed. Sea level measured from tide gauges are called Relative Sea Level, since tide gauge measurements are relative to the benchmark tied to the Earth's crust [1]. The term Absolute Sea Level, on the other hand, is sea level referred to the geocentric reference frame [2]. For the purposes of this study, net Absolute Sea Level Change (ASLC) will be used to refer to sea level change referred to a geocentric reference frame corrected for Vertical Land Motion (VLM). Vertical Land Motion refers to the change in elevation of land due to either natural or man-made causes.

There are currently 4.3 million people in the Philippines living below the high tide line, and by 2050, if the high greenhouse gas emissions continue, this will rise to about 6.8 million people [3]. The Philippines also has the highest damage cost associated with sea level rise (US $6.5 billion/year) among the countries of the Coral Triangle (Indonesia, Malaysia, Philippines, East Timor, Papua New Guinea, and Solomon Islands) [4]. Thus, investigating the sea level change can help in the planning for the mitigation of the risks due to sea level rise.

In Marinduque, Philippines, active faults cause tectonic activities evidenced by earthquakes recorded by USGS and PHIVOLCS which contribute to the VLM in the area, and thus affecting the sea level readings from the tide gauge. Due to these reasons, this research studies the relative and net ASLC in Mogpog, Marinduque using tide gauge data, Global Navigation Satellite System (GNSS) data, and Interferometric Synthetic Aperture Radar (InSAR) techniques, particularly Persistent Scatterer InSAR (PSInSAR). The general objective of this research is to introduce an alternative to geodetic leveling from a nearby GNSS stations for correcting tide gauge readings for VLM by Persistent Scatterer Interferometric Synthetic Aperture Radar (PSInSAR) derived VLM to estimate the net absolute sea level change in Mogpog, Marinduque.

II. METHODS FOR QUANTIFYING ABSOLUTE SEA LEVEL CHANGE

2.1. Satellite Altimeter

Absolute sea level can be measured by using satellite altimetry [5], [6]. Satellite altimetry works by pointing an electromagnetic wave (EM) at nadir direction. The distance between the satellite and the surface, can be computed using Eq. (1)

$$d = vt \quad \text{(Eq. 1)}$$

Where "d" is the distance between the satellite and the surface, "v" is the speed of propagation of the EM wave which is equal to the speed of light, and "t" is the duration of the one-way trip of the transmitted EM wave as it was sent by the sensor [7].

Altimeter data should be corrected to consider instrumental, atmospheric, and geophysical effects that can affect its accuracy. Measurements near coasts are also affected by land contamination [8] (i.e. radar signals near the coast can have complex waveform as compared to the usual open-sea footprint which reduces the accuracy of the measurement.) Scientists studying sea level using altimeters devised "Retrackers" to correct altimeter measurements from land contamination like "ALES: Adaptive Leading Edge Subwaveform retracker", developed by Passaro et al. [9]. ALES uses a part of returned radar echo and analyze it with the expected "open-ocean" waveform to correct for the distortion caused by land contamination.

2.2 Tide Gauge and GNSS

Measurements of sea level provided by tide gauges are affected by signals from land motion. Thus, VLM should be removed from the measurements, to obtain the net ASLC from tide gauges. According to Filmer et al. [10], the conventional method for monitoring VLM between tide gauge and the nearest GNSS station is by repeat differential levelling. For the Philippines, the tide gauges are either collocated with a cGNSS receiver or connected to a benchmark by differential levelling. For tide gauges with cGNSS receivers, different studies derived VLM using collocated GNSS receivers [11], [12], [13], [14]. An example of such is the study of Bitharis et al. [12] where the researchers processed tide gauge and GNSS data to correct estimates of sea level rise from tide gauges by accounting for VLM. Corrected sea level trend was computed using Eq. (2) [12].

$$U^{abs} = H + h \quad \text{(Eq. 2)}$$

Where U^{abs} is the net absolute (corrected geocentric) sea level trend, H is the local sea level trend from tide gauge, and h is the VLM correction rate. Assuming that their measurements are uncorrelated, the uncertainties were computed using Eq. (3) [12].

$$\sigma^{abs} = \sqrt{\sigma_H^2 + \sigma_h^2} \quad \text{(Eq. 3)}$$

where σ^{abs} is the uncertainty of the absolute sea level trend, and σ_H and σ_h are the uncertainties of the local sea level trend and VLM rate, respectively.

2.3 Tide Gauge and InSAR

VLMs are primarily caused by tectonic and volcanic activities. Studies have been conducted on the correction of sea level rise derived from tide gauge stations using GNSS data due to earthquake induced land motion [15], [16], [17], [13]. Human activities can also induce land subsidence through groundwater and hydrocarbon extraction [18]. VLM can be obtained from InSAR by utilizing at least a pair of radar images to produce an interferogram which shows the difference in phase between the two images, along the line of sight of the satellite.

A study by Raucoules et al. [2] investigated urban ground motion in Manila using Differential Interferometric Synthetic Aperture Radar (DInSAR) and its implication in sea level change studies. In the said research, extraction of absolute sea-level using nearby GNSS stations was not possible in their area of interest because the nearest GNSS station from the tide gauge station is several kilometers away. The result of the study further showed that the tide gauge and GNSS stations experience different ground motions. VLM can be removed from the tide gauge measurements using a nearby GNSS station if the tide gauge and GNSS station experiences the same VLM and the motion is linear (i.e. no tectonic and volcanic activity) [2].

2.4 Persistent Scatterer Interferometric Synthetic Aperture Radar (PSInSAR)

InSAR utilizes the difference in phase values between two SAR images acquired from a different look or time. As described in Crosetto et al. [19], InSAR is given by the equation:

$$\Delta\varphi_{int} = \varphi_f - \varphi_i = \frac{D_f - D_i}{\frac{\lambda}{4\pi}} + \varphi_{scatt,f} - \varphi_{scatt,i} \quad \text{(Eq. 4)}$$

where:

$\Delta\varphi_{int}$ = Difference of the phases between the initial and final SAR acquisition
φ_f , φ_i = Phases of the final and initial SAR acquisition
D_i , D_f = Distance between the satellite and target from initial and final acquisition
$\varphi_{scatt,f}$, $\varphi_{scatt,i}$ = Phase shift due to the interaction between the radar and target

Eq. (4) describes an equation for generation of Digital Elevation Model (DEM). The first term describes the topographic phase component. For measuring displacements, an additional term is added to account for the movement of the target as seen in Eq. (5).

$$\Delta\varphi_{int} = \varphi_f - \varphi_i = \frac{D_f - D_i}{\frac{\lambda}{4\pi}} + \frac{D'_f - D_f}{\frac{\lambda}{4\pi}} + \varphi_{scatt,f} - \varphi_{scatt,i} \quad \text{(Eq. 5)}$$

D'$_f$ represents the displacement of the point target after the first image acquisition. The topographic phase component can be removed from the equation using a DEM containing the scene of the image. A more complex version of Eq. (5) includes the effects of atmosphere and orbital errors.

For validation of InSAR measurements, the measurements must be validated in Line-of-Sight (LOS) measurements instead of projected vertical measurements as suggested by Fuhrmann & Garthwaite [20]. Deformations are inherently measured along the satellite's Line-of-Sight (LOS) since SAR sensors are pointed at an angle with respect to nadir. Projecting InSAR measurements into vertical measurements introduces an error given by the equation:

$$\Delta v_{u,proj,max} = v_u - v_{u,proj} = tan(\theta) v_{H,max} \quad \text{(Eq. 6)}$$

where:

v_u = True vertical deformation/velocity
$v_{u,proj}$ = Projected vertical deformation/velocity from LOS measurements
Θ = Incidence angle of the SAR geometry
$v_{H,max}$ = Maximum horizontal deformation/velocity

III. METHODOLOGY

3.1 Study Area

Marinduque is part of the Southwestern Tagalog Region (MIMAROPA), Philippines located between 121.79° E to 122.17° E, and 13.58° N to 13.19° N (Figure 1). It is to the north of Romblon, east of Mindoro, and west of Quezon province.

The Municipality of Mogpog in Marinduque was chosen as the study area due to the lack of collocated GNSS receiver at the tide gauge station, and the availability of data.

The locations of the Balanacan Tide Gauge (TG) Station; PMOG Active Geodetic Network (AGN) Station; and Station Balanacan, the reference point of the Luzon Datum of 1911, are

shown in Figure 1. Inset maps on the left side of Figure 1 shows the vicinity of each station for better understanding of the stations' surroundings. Balanacan TG Station and PMOG AGN Station are approximately six (6) kilometers apart from each other.

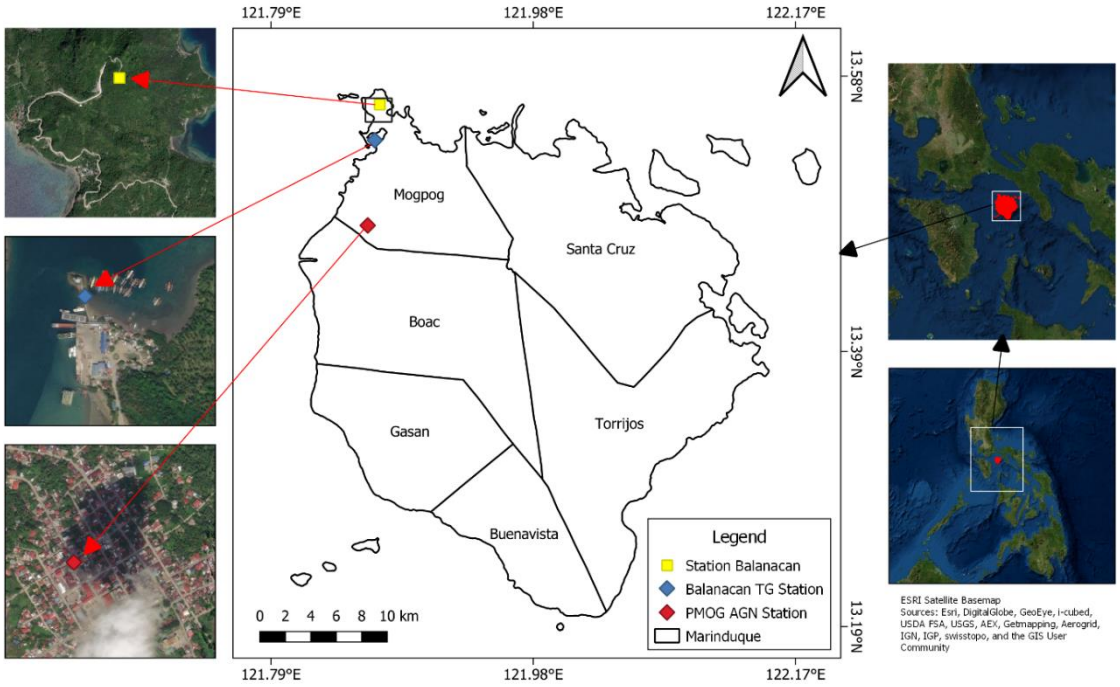

Figure 1. Study area

The active faults located in Marinduque are Central Marinduque Fault, North Marinduque Fault, and the Philippine Fault; and a potential active fault, Malindig fault as seen in Figure 2.

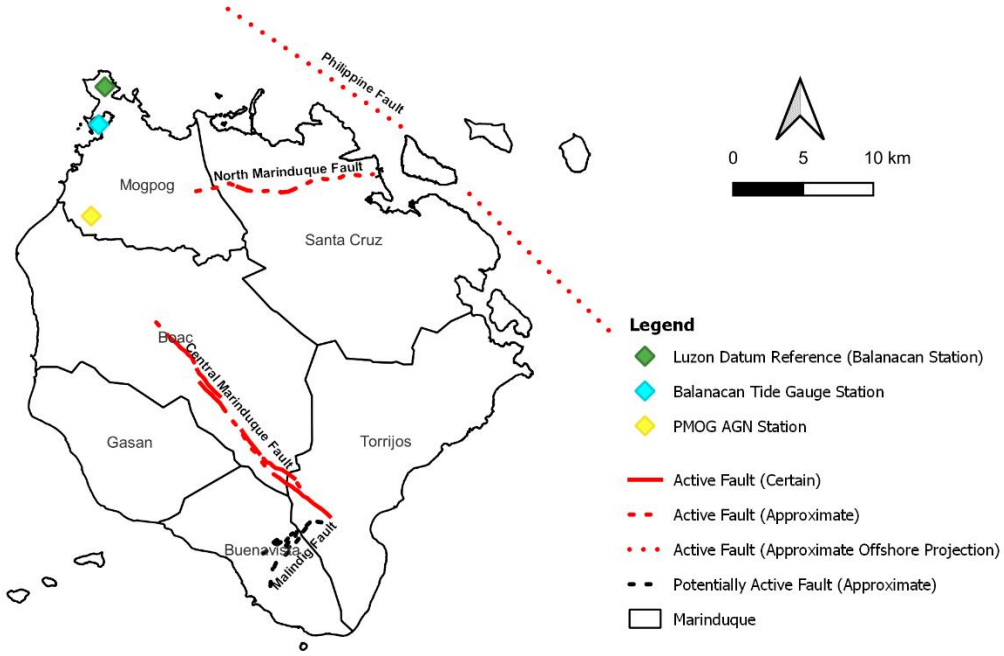

Figure 2. Active Faults in Marinduque [21]

3.2 Data

3.2.1 Tide Gauge Data

The Balanacan Tide Gauge Station located in Mogpog, Marinduque was established in 2007. Hourly sea level data of the said tide gauge for years 2007-2020, and the values needed for the conversion of readings to WGS84 were acquired from the National Mapping and Resource Information Authority (NAMRIA). For the data gaps in the tide gauge data in 2018, NAMRIA provided predicted tides for the time periods which overlapped with the SAR Data.

3.2.2 GNSS Data

Daily post-processed GNSS data of the Active Geodetic Network (AGN) Station - PMOG in Mogpog, Marinduque from 2014 to 2019 were provided by NAMRIA in Earth-Centered, Earth-Fixed (ECEF) coordinates. The PMOG AGN Station was established in 2014 with coordinates 13.47°N, 121.86°E, and 64.533 m.

3.2.3 SAR Data

SAR images from the Sentinel-1 mission were used for the study due to its availability. Sentinel-1 utilizes C-band Synthetic Aperture Radar which can map the Earth's surface any time of the day and during any weather conditions [22]. Sentinel-1 Interferometric Wide (IW) swath Single Look Complex (SLC) images with 24 days interval were downloaded from the Alaska Satellite Facility (ASF) (https://search.asf.alaska.edu). The characteristics of the downloaded images are tabulated in Table 1.

Table 1. Characteristics of the downloaded Sentinel-1 data

Pass Direction	Number of Scenes	Path	Frame	Mean Incidence Angle	Satellite Heading Angle	Date of First Image	Date of Last Image
Ascending	47	142	39	43.9533°	-169.0697°	December 09, 2016	December 18, 2019
Descending	46	134	545, 550	44°	-11.009°	December 14, 2016	December 11, 2019

3.3 Processing

The general flow of the methodology can be seen in Figure 3 below wherein it was divided into the processing of the different datasets, validation of PSInSAR results, and extraction of vertical land motion and net absolute sea level change.

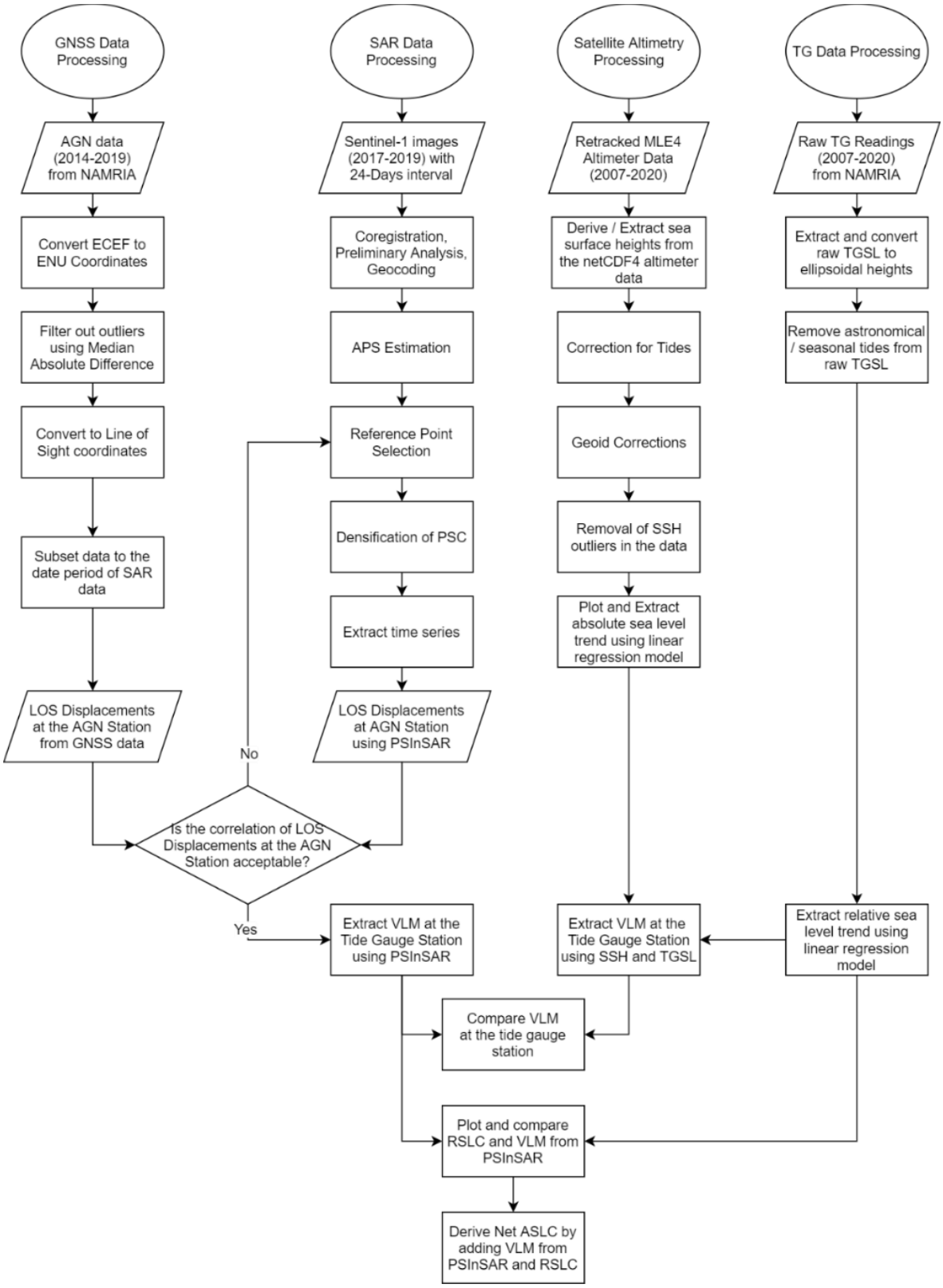

Figure 3. Processing flow of the study

3.3.1 PSInSAR Processing

The ascending and descending data were coregistered and processed for PSInSAR, separately using SARPROZ. SARPROZ is a software based on MATLAB that implements SAR, InSAR processing, and Multi-temporal InSAR processing techniques [23]. For both ascending and descending, the VV polarization and the sub-swath containing the study area were extracted and precise orbits were applied. The images were then coregistered using the master images (Figure 4) acquired on March 29, 2019, and February 26, 2019 for ascending and descending, respectively.

Preliminary analysis and geocoding needed for the succeeding PSInSAR analysis were performed. This includes the generation of the reflectivity map and computation of amplitude stability index (ASI), selection of Ground Control Point (GCP), and calculation of external DEM and synthetic amplitude in SAR coordinates. The GCPs for both the ascending and descending data were automatically selected by the software by means of keeping the orbit offsets since precise orbits were already used in the coregistration of images. Orbit offsets refer to the parameters radar images have which is important for geometric correction. The default DEM used for processing was SRTM.

Eq. (7) describes the equation for the ASI threshold which was used to select possible Permanent Scatter Candidates (PSC). The higher value, the stricter in selection of points. PSInSAR processing was performed by selecting points with ASI greater than or equal to 0.73 for ascending and 0.75 for descending, as PSCs. Lower ASI threshold was set for the ascending data as it has a lower number of PSC for the same threshold as compared with descending images.

$$ASI = 1 - (\sigma_a \,/\, \underline{a}) \qquad \text{(Eq. 7)}$$

where $\underline{a}$ is the mean amplitude and σ_a is the standard deviation of amplitude in time.

Connections between the PSCs were generated using the Delaunay triangulation. These connections were processed using a linear model while taking into account thermal expansion to estimate unknown parameters such as velocity and height. The ambient temperature data used was acquired from the National Oceanic and Atmospheric Administration's National Center for Environmental Information (NOAA's NCEI) and was measured at Calapan, Oriental Mindoro, the nearest weather station from Marinduque [24]. An assumed stable reference point with high temporal coherence was manually selected (Figure 4), where the measurements of the PSCs will be referred. This meant that analysis from both satellite geometries are assured to be measured from the same area and contamination of velocity rates may be reduced. The atmospheric phase screen (APS) is then estimated by inverting the phase residuals produced after removing the previously estimated linear model. APS is one of the major sources of errors for radar images due to the effects of the atmosphere on the emitted radar signal.

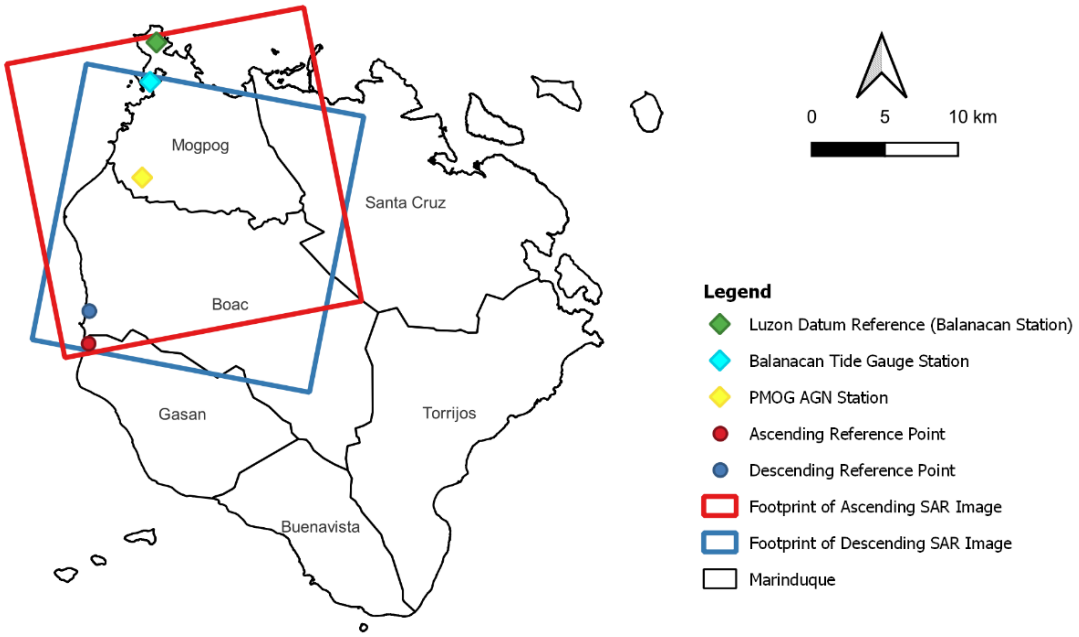

Figure 4. Footprint of the SAR images for ascending (red box) and descending (blue box), including points of interests

After the estimation of APS, the ASI threshold was lowered to 0.67 for ascending and 0.7 for descending in order to densify the selected points. The new set of points were reprocessed using the same reference point, and the range of the parameters were adjusted accordingly. Lastly, the PSInSAR time series containing the derived Line-of-Sight (LOS) cumulative displacements was exported.

3.3.2 GNSS Data Processing

Since the GNSS data acquired from NAMRIA are in ECEF coordinates and will be used to validate PSInSAR results, the data were converted into East-North-Up (ENU) coordinates for further processing and analysis. After conversion, the outliers are filtered out using Median Absolute Difference (MAD) with a threshold of 2.5. Selection of the threshold was based on three values (3, 2.5, 2) where higher number represents a conservative filtering while lower number represents stringent filtering [25].

Khorrami, et al. [26] and Fuhrmann & Garthwaite [20] suggested that validation of PSInSAR using GNSS data must be in Line-Of-Sight (LOS) geometry because conversion of PSInSAR from LOS geometry to East-Up introduces errors. Thus, GNSS data were converted from ENU to LOS displacements using Eq. (8). For comparison and validation with the PSInSAR results, the LOS converted GNSS data were then resampled into 24-days.

$$GPS_{LOS} = (GPS_{UP} * cos(\theta_{inc})) - (GPS_{NORTH} * cos(\alpha_{azimuth} - \frac{3\pi}{2}) * sin(\theta_{inc})) - (GPS_{EAST} * sin(\alpha_{azimuth} - \frac{3\pi}{2}) * sin(\theta_{inc})) \quad \text{(Eq. 8)}$$

where:

θ_{inc} = Incidence angle of the satellite

$\alpha_{azimuth}$ = Satellite heading/azimuth or the flight direction of the satellite reckoned from the north

3.3.3 *Tide Gauge Processing*

Eq. (9) was used to change the datum of raw tide gauge readings from an arbitrary datum, 0TS, to a known vertical datum, WGS84.

$$TGSL_{ellipsoidal} = (h_{TGBM} - h_{TGBM/0TS}) + TGSL_{0TS} \quad \text{(Eq. 9)}$$

where $TGSL_{ellipsoidal}$ is the ellipsoidal tide gauge readings, $h_{TGBM}$is the ellipsoidal height of the tide gauge benchmark (TGBM), $h_{TGBM/0TS}$ is the height of the TGBM referred to 0TS, and $TGSL_{0TS}$is the raw tide gauge readings.

Erroneous data, outliers, and the effects of astronomical tides were removed from the tide gauge readings before further processing. Raw erroneous measurements were measurements recorded by the tide gauge as "999". Outliers in tide gauge readings were removed visually after plotting the time series as a scatterplot. Outliers were characterized as points in the plot that has an approximate amplitude difference of greater than five meters than the rest of measurements. Linear regression was then applied to the corrected tide gauge readings to obtain the relative sea level trend.

3.3.4 Validation of the PSInSAR results

GNSS data at the AGN Station were used to validate the PSInSAR results as previously done by Khorrami, et al. [26]. For both ascending and descending PSInSAR results, points within 50-meter radius of the AGN Station were extracted and their average displacements throughout the time series were calculated.

The PSInSAR Line-of-sight (LOS) displacements at the AGN Station were correlated with the LOS converted GNSS data resampled to 24-days, to match the acquisition dates of the SAR images used, from December 2016 to May 2019. Root Mean Square Error (RMSE) was also computed using the same data, to measure the difference between the two datasets. If the correlation for both ascending and descending PSInSAR results and the LOS converted GNSS data reach the acceptable correlation, the PSInSAR results can be used for determining the VLM near the Balanacan tide gauge station since there are no collocated cGNSS near it; otherwise, PSInSAR processing will be repeated by selecting a new reference point.

3.3.5 *Computation of VLM at the Tide Gauge Station*

After the validation of the PSInSAR results using GNSS data, extraction of persistent scatterer (PS) points near the tide gauge station was performed using QGIS. 1km buffer radius around the tide gauge for descending, and 50m buffer radius around the center of the nearest town south of the tide gauge station for ascending were used to extract the said points. The difference in extraction areas between descending and ascending PSInSAR results was due to the lack of reliable PS points near the tide gauge station on ascending images.

The extracted PS points near the tide gauge station were then converted into vertical components using Eq. (10).

$$\begin{bmatrix} d_{asc} \\ d_{des} \end{bmatrix} = \begin{bmatrix} cos\theta_{asc} & -cos\alpha_{asc}sin\theta_{asc} \\ cos\theta_{des} & -cos\alpha_{asc}sin\theta_{asc} \end{bmatrix} \begin{bmatrix} d_{ver} \\ d_{hor} \end{bmatrix} \quad \text{(Eq. 10)}$$

where θ represents the local incidence angle and α is the satellite heading/azimuth or the flight direction of the satellite reckoned from the north.

3.3.6 Computation of the Net Absolute Sea Level at the Tide Gauge Station

The computed VLM rate from PSInSAR and the sea level rates from the processed tide gauge data were used to compute the ASLC at the tide gauge station using Eq. (2). Due to different time periods of SAR images (2016-2019) and tide gauge measurements (2007-2020), VLM rate from PSInSAR were assumed to be constant throughout 2007 to 2020. The results were tabulated in Table 3.

IV. RESULTS AND DISCUSSIONS

4.1. PSInSAR Line-of-Sight (LOS) and Vertical Velocities

The coherence of PS points in ascending and descending are displayed in Figures 5a and 5b. PS points with coherence lower than 0.6 for ascending, and 0.75 for descending are filtered out. The difference in the threshold used for exporting PS points was due to the result of descending images detecting more PS points than the result of ascending images. The PS points around the AGN Station, that were used for correlation with the GNSS observation, have good coherence (0.8 to 1) for both ascending and descending. The same can be observed with the PS points near the tide gauge station.

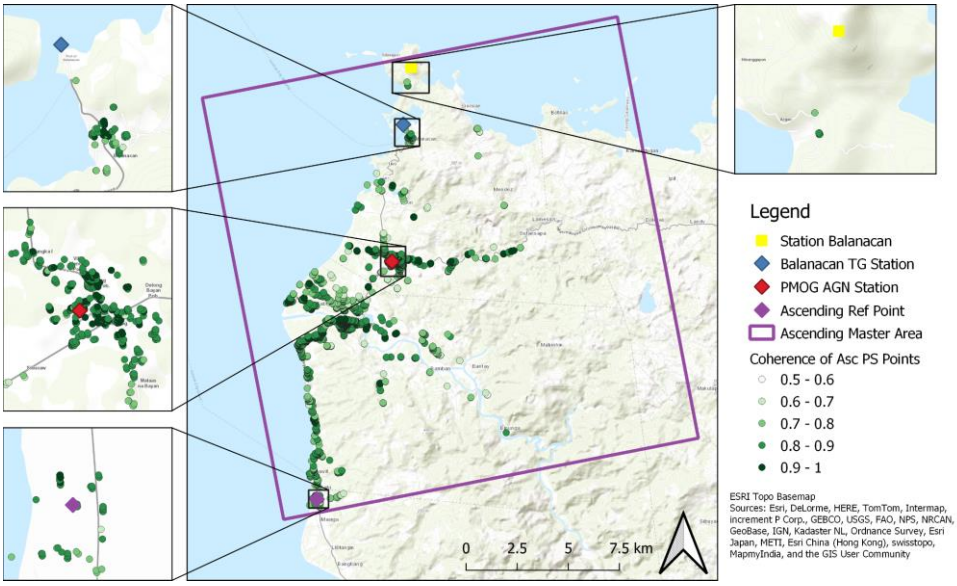

Figure 5a. Coherence of PS Points in the Ascending Geometries

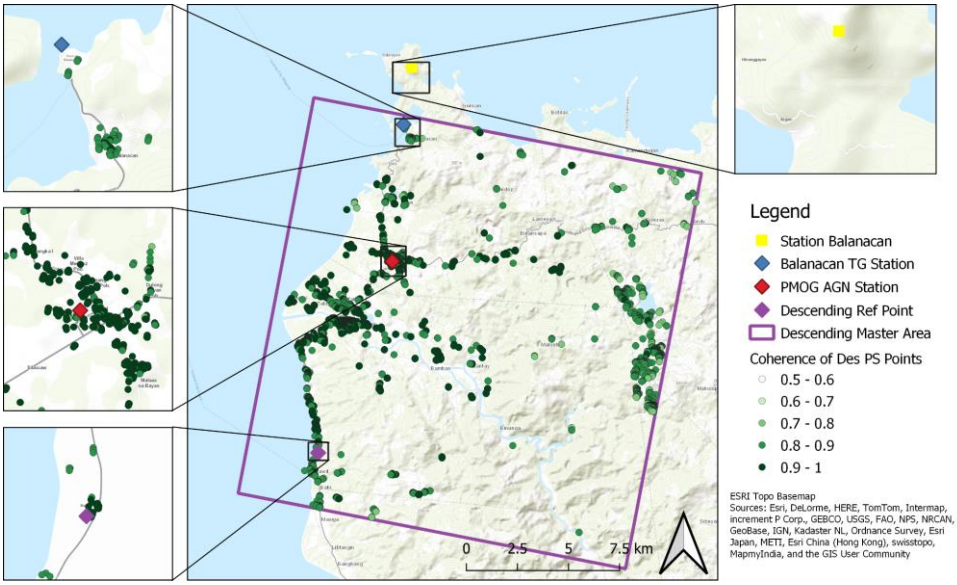

Figure 5b. Coherence of PS Points in the Descending Geometries

The LOS and vertical velocities of the PS points obtained from PSInSAR processing can be seen in Figure 6. The velocities in the ascending and descending geometry are measured along the LOS of the satellite. The bigger arrow in Figures 6a and 6b are the direction of the flight of the satellite, or the satellite heading, while the smaller arrow is the look direction of the sensor.

All of the 2410 PS points in the result of ascending geometry have a negative velocity ranging from -10 to 0 mm/yr (Figure 6a) while in descending, 3714 out of 3975 PS points have positive velocities with values ranging from 0 to 5 mm/yr (Figure 6b). Positive velocity in LOS

geometry means that points are moving towards the satellite along LOS, and the opposite for negative velocity. Due to the differing areas covered by ascending and descending images, only ascending images covered the location of Station Balanacan and its neighboring areas. Moreover, due to the lack of built-up areas, there were no immediate PS points near Station Balanacan. The nearest PS points are located around 1km from Station with an average LOS velocity of -5.486 mm/yr.

Interpretation of land motion using LOS velocities presents a challenge since it is based on satellite geometry and not on the conventional ENU geometry; hence, the LOS velocities were converted to vertical velocities (Figure 6c) using Eq. (10). In the figure, vertical velocities are ranging from -5 to 5 mm/yr. An average of 0.708mm/year of land subsidence was observed in Barangay Poblacion of Mogpog where PMOG AGN station is situated.

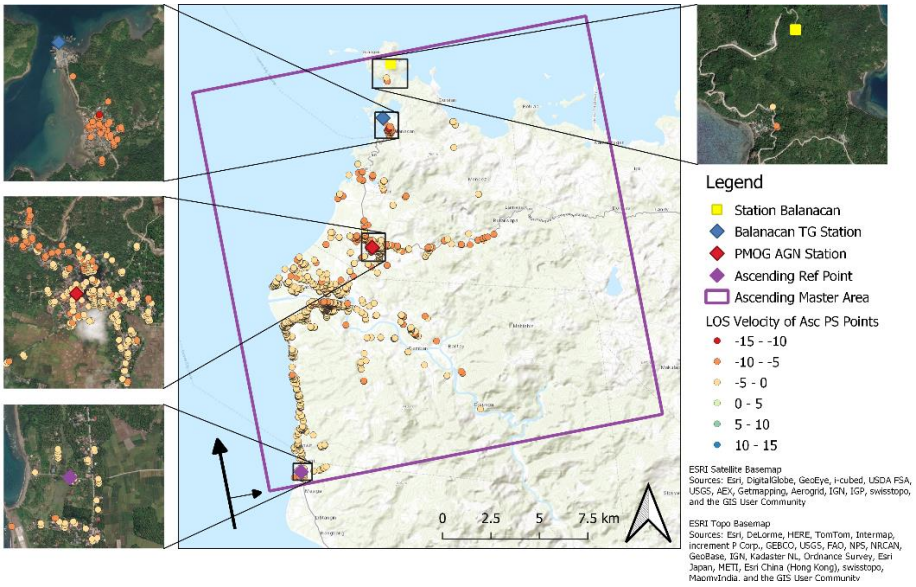

Figure 6a. Ascending Velocities of the PS points in mm/yr

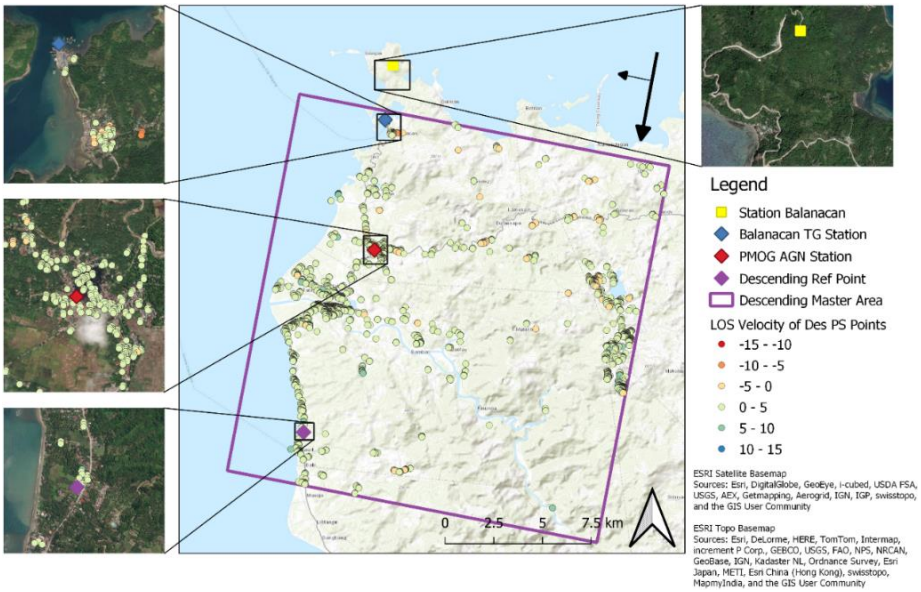

Figure 6b. Descending LOS Velocities, Velocities of the PS points in mm/yr

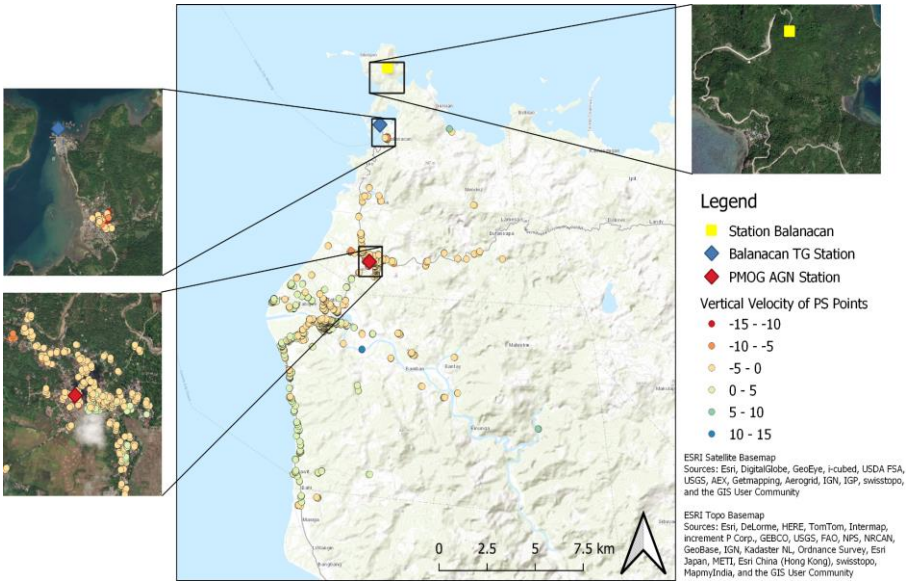

Figure 6c. Vertical Velocities of the PS points in mm/yr

4.2. GNSS ENU and LOS Displacements

The displacements after converting the GNSS data from ECEF to ENU coordinates, and filtering the outliers are shown in Figure 7. The GNSS ENU displacements were then converted to ascending and descending LOS displacements using Eq. (8) seen in Figure 8.

The trends of the displacements were computed in two time periods: 1) from start of GNSS observation (August 2014) to May 2019; and 2) period of GNSS observation matching the SAR image acquisition (December 2016 to May 2019). Although the SAR data available is up

to December of 2019, the subset taken was only up to May of 2019 since according to NAMRIA, GNSS data after May of 2019 indicated data jumps that still need verification.

The trend of the North-South (N-S) displacements is positive while the East-West (E-W) is negative, indicating that the area where PMOG AGN Station is located is moving in a North-West direction. Vertical movement shows a seasonal trend visible on both the whole and subset GNSS data. This may have been caused by the location of the AGN station, as it is located on top of a building structure. Although there were no spikes or indication of movement due to earthquakes with high magnitude in the time series, the trend of N-S and E-W displacements indicated that the area where the AGN is located is moving at a rate of 10.785 mm/yr in N 58.57° W direction. When converted to LOS (Figure 8), the trend of the displacements in the ascending is negative and positive in the descending.

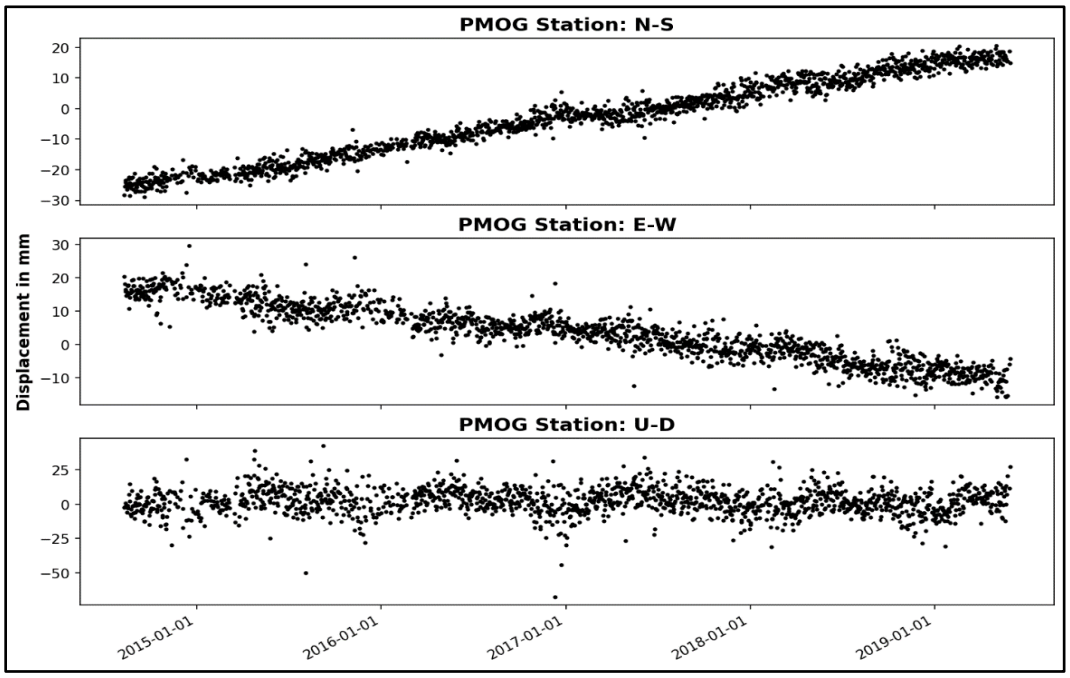

Figure 7a. Daily GNSS North-South, East-West, and Up-Down displacements from 8/2014-5/2019 after removing the outliers. North-South Rate: 9.208 ± 0.038, East-West Rate: -5.624 ± 0.054, Up-Down Rate: -0.404 ± 0.173

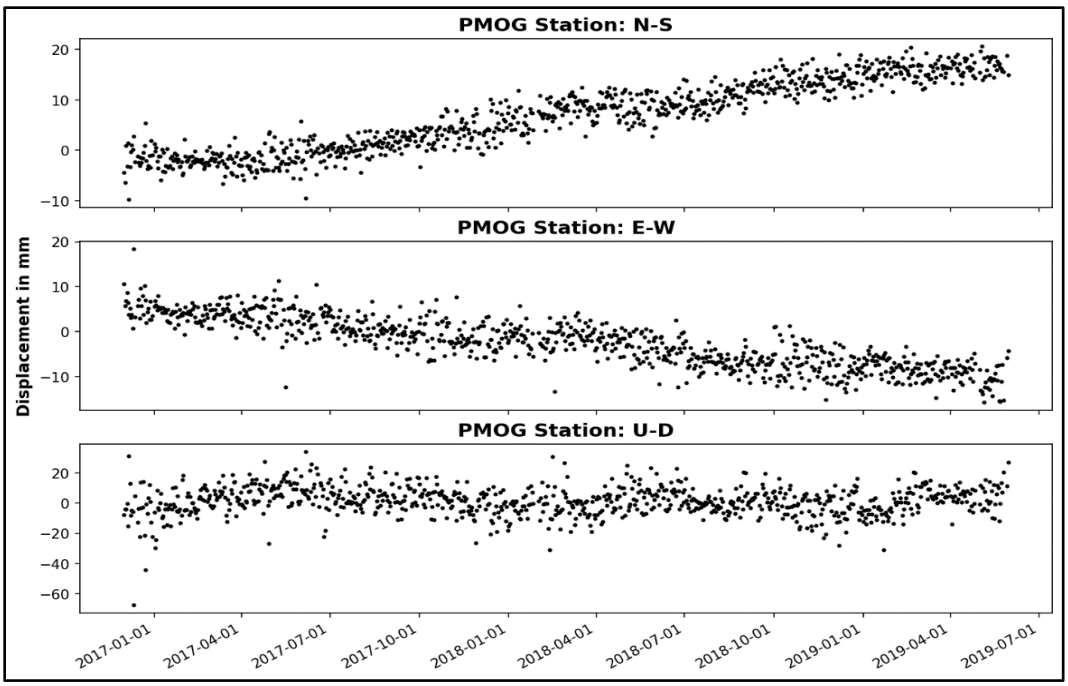

Figure 7b. Daily GNSS North-South, East-West, and Up-Down displacements from 12/2016-5/2019, after removing the outliers. North-South Rate: 9.044 ± 0.105, East-West Rate: -6.484 ± 0.131, Up-Down Rate: -0.591 ± 0.450

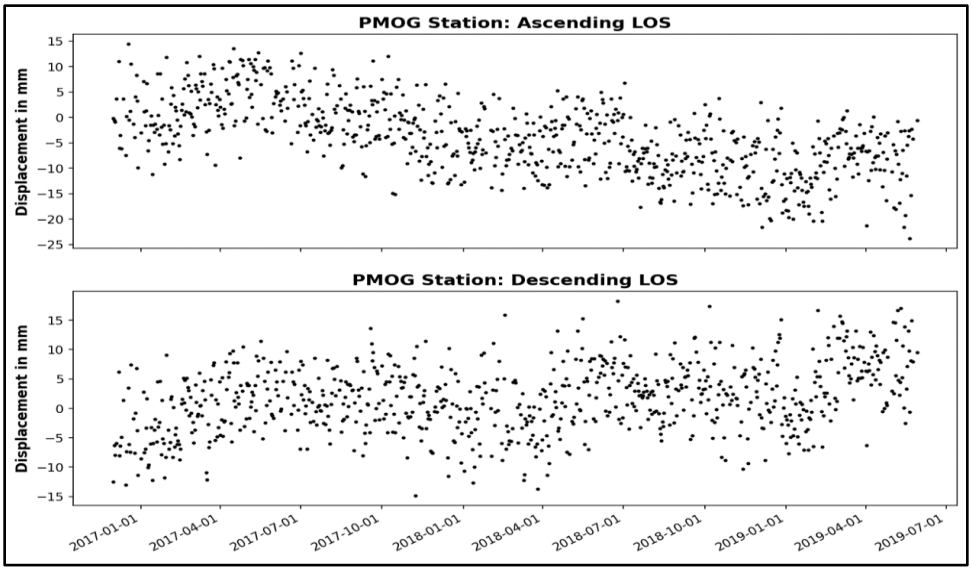

Figure 8. Daily GNSS Ascending and Descending Line-of-Sight Displacements 12/2016-5/2019

4.3. PSInSAR Results Validation using GNSS Data

To validate the results of the PSInSAR processing, the average LOS displacements of PS points within 50-meter radius of the AGN Station were compared with displacements from the GNSS data (Figures 9 and 10). To compare the displacements, the GNSS LOS data was resampled into 24-days (Figure 10).

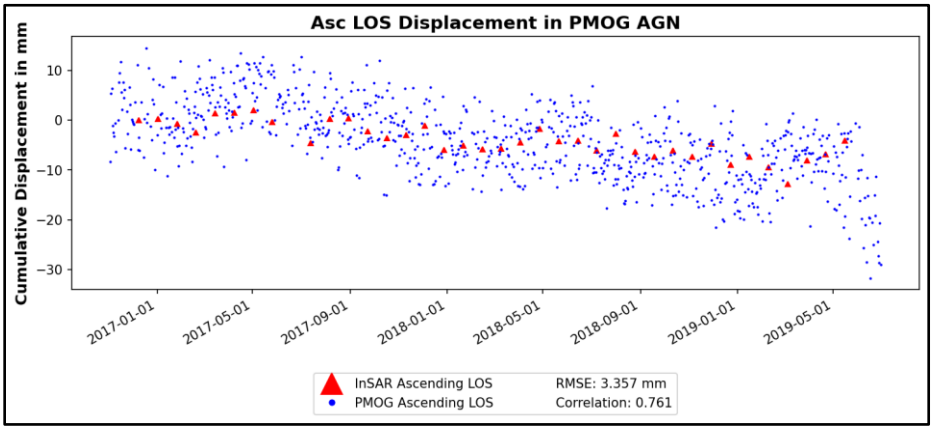

Figure 9a. PSInSAR (red) and Daily GNSS (blue) LOS Displacements at the PMOG AGN Station in Ascending from 12/2016-5/2019

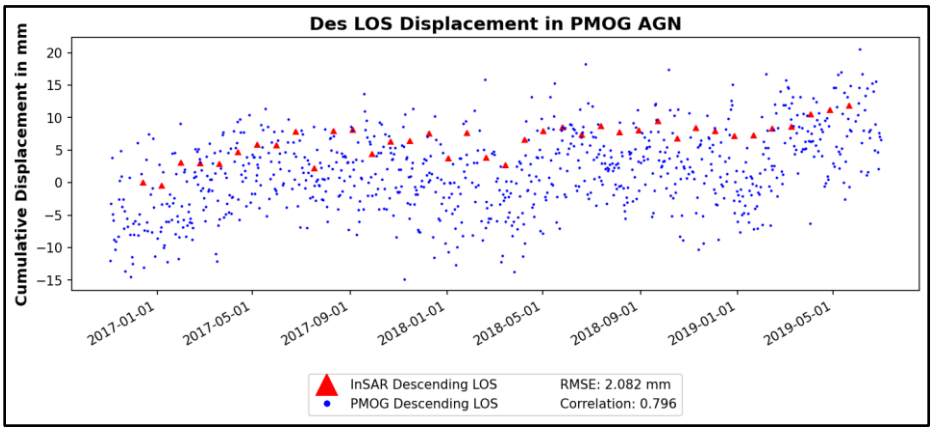

Figure 9b. PSInSAR (red) and Daily GNSS (blue) LOS Displacements at the PMOG AGN Station in Descending from 12/2016-5/2019

Looking at Figures 9 and 10, the LOS displacements from ascending and descending geometries have a Root Mean Square Error (RMSE) equal to 3.357 mm and 2.082mm respectively. The correlations of each geometry compared to LOS converted PMOG AGN station were equal to 0.761 and 0.796 respectively. According to Din et al. [1], a correlation between 0.7 to 0.9 means that there is a strong relationship between the displacements from the PSInSAR and GNSS LOS data (Table 2). Since the PSInSAR LOS results have a strong correlation with the LOS-converted GNSS data from Figures 8 and 9, the PSInSAR computed

vertical deformation near the tide gauge can be used in the absence of a collocated GNSS receiver.

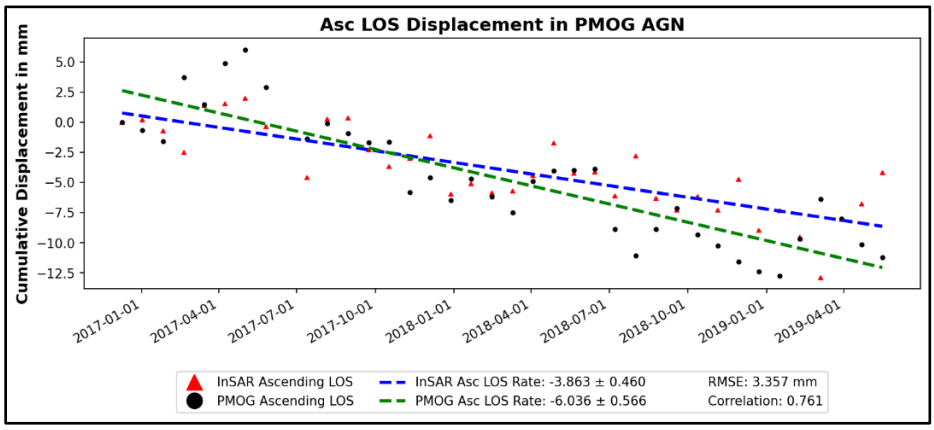

Figure 10a. PSInSAR (red) and Resampled GNSS (blue) LOS Displacements at the PMOG AGN Station in Ascending from 12/2016-5/2019

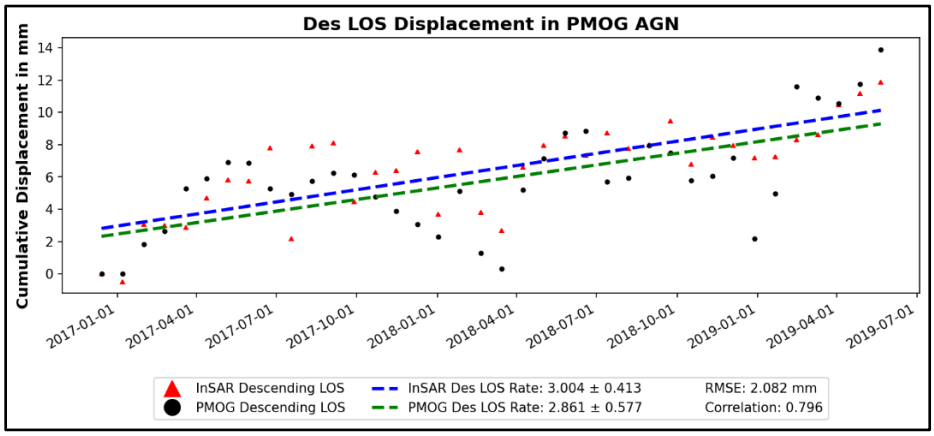

Figure 10b. PSInSAR (red) and Resampled GNSS (blue) LOS Displacements at the PMOG AGN Station in Descending from 12/2016-5/2019

Table 2. Descriptions of Correlation Coefficients

Correlation	Description
1	Perfect
0.7 - 0.9	Strong
0.4 - 0.6	Moderate
Less than 0.3	Weak

Figures 11a and 11b shows the comparison between the vertical and horizontal displacements converted from the LOS PSInSAR result using the Eq. (10), and the displacements from GNSS data at PMOG Station. The plots proved conversion of PSInSAR

results introduces errors especially in vertical component as given in Eq (6). Although the correlation is low between PSInSAR and GNSS vertical component time series, their rates are almost the same. East-West component have a higher correlation with each other, but the velocity has a higher difference. Moreover, both PSInSAR and GNSS data are in agreement that the area is moving to the west and experiencing slow subsidence.

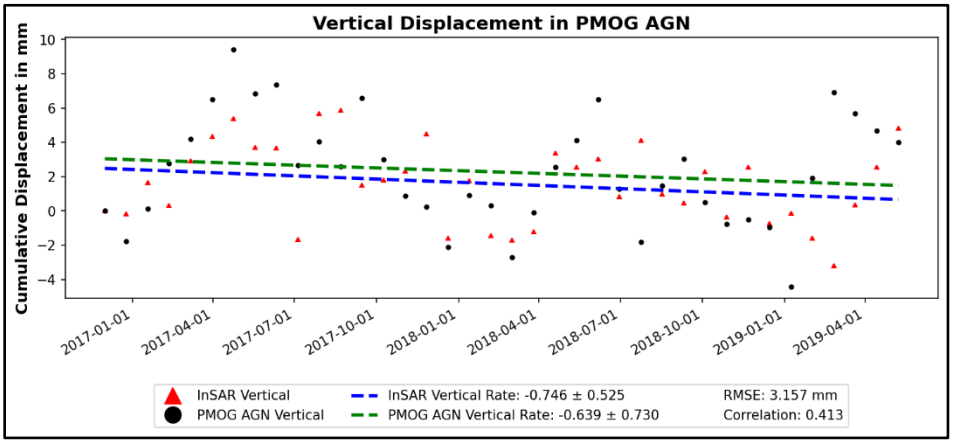

Figure 11a. Comparison of Displacements at PMOG AGN Station for Vertical component

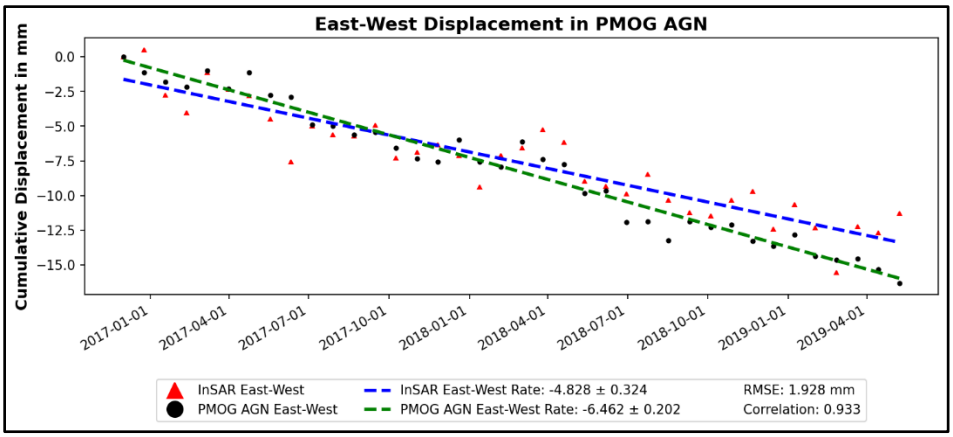

Figure 11b. Comparison of Displacements at PMOG AGN Station for Horizontal component

4.4. Vertical and Horizontal (East-West) Displacements at the Tide Gauge Station

The vertical and horizontal displacements at the tide gauge station from the PSInSAR results computed from using Eq. (10) can be seen in Figures 12 and 13, respectively. The rate of the vertical displacement at the tide gauge station is -3.822 ± 0.713 mm/yr while the horizontal displacement rate is -7.408 ± 0.684 mm/yr. Due to the inherent flight direction of satellites, being almost polar orbits or sun-synchronous as indicated by satellite heading angle in Table 1 and only two different SAR geometries were used, horizontal displacements derived from satellite images are poorly constrained in North-South direction based on Eq. (8) [20]. Thus, North-South displacements at the tide gauge station were excluded from the results.

Moreover, Khorrami et al. [26] assumed North-South displacement to be negligible as SAR images are less sensitive to the North-South component of deformation.

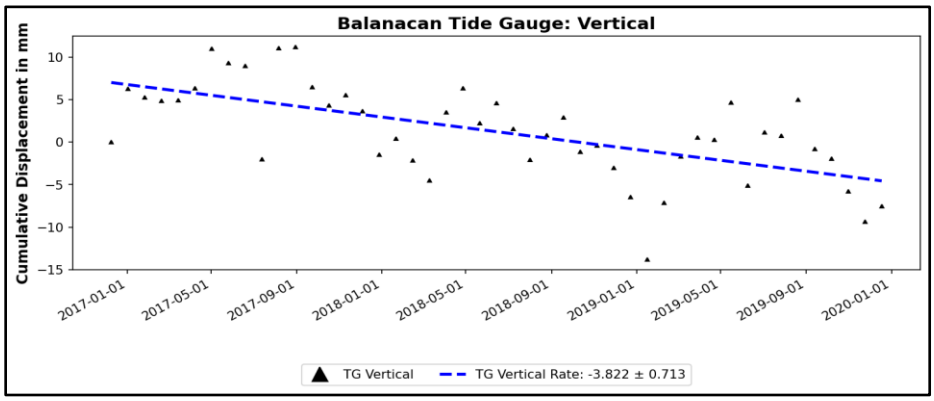

Figure 12. Vertical Displacements at the Tide Gauge Station from PSInSAR

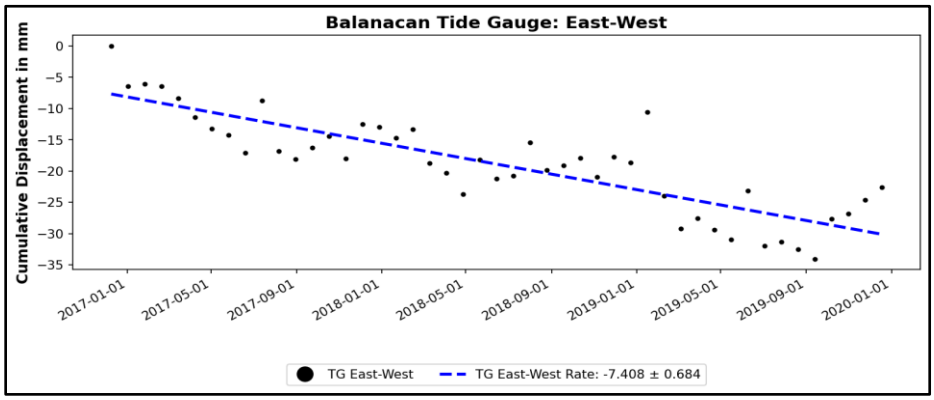

Figure 13. East-West Displacements at the Tide Gauge Station from PSInSAR

4.5. Tide Gauge Sea Level

The hourly ellipsoidal tide gauge sea level (TGSL) of the Balanacan tide gauge station from December 2007 to December 2020 was plotted in Figure 14. Gaps in the TGSL were caused by downtime of the tide gauge. The TGSL rate during the said period is 0.23 ± 0.63 mm/yr. The TGSL rate contains signals from both sea level change and VLM. Based on the results of CSLR [6], sea level change from satellite altimetry, which measures oceanic/coastal sea level heights directly, recorded a decrease in sea level change around the coastal waters near the tide gauge station for the same period. Thus, may indicate that tide gauge station experiences subsidence based on the Eq. (2).

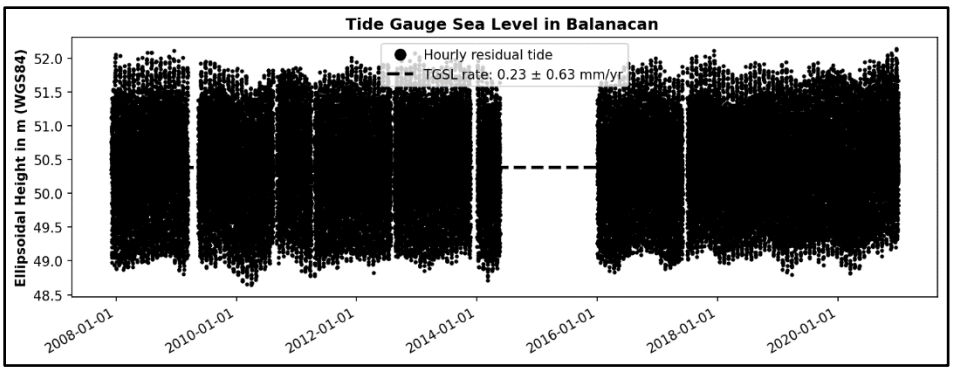

Figure 14. Hourly Tide Gauge Sea Level at the Balanacan Station from 12/2007-12/2020

4.6. Estimated Net Absolute Sea Level Change Rate

The estimated rate of net absolute sea level change computed using Eq. (2) is equal to -3.592 ± 0.951 mm/yr (Table 3). Due to the land subsidence experienced by the tide gauge as observed from PSInSAR, the tide gauge records an increase in sea level (positive TGSL rate), even though the estimated rate of absolute sea level change indicates decrease in sea level. The occurrence of VLM masked the true sea level trend in the area. The negative net absolute sea level trend observed was due to the influence of El Niño based on the technical report of CSLR-Phil [6]. According to Behera et al. [27]:

El Niño is referred to the abnormal ocean warming that develops once in a few years in the eastern tropical Pacific Ocean. The warming covers a large part of central tropical Pacific and linked to variations in the atmospheric circulations and oceanic conditions.

Except for El Niño years, sea surface temperatures (SSTs) off Peru and tropical South America are normally cooler than its western counterpart even though both sides are in the same latitude band receiving almost the same amount of incoming solar radiation (p. 61).

Aside from changes to the normal sea surface temperatures between East and west Pacific, El Niño is also characterized by sea level fall in the west Pacific and rise in the east as much as 25 cm due to the surge of warm water to the east Pacific along the equator [28].The same trend was manifested by most tide gauges with the same period of observation between 2007/2008 to 2019 [6].

Table 3. Net Absolute Sea Level Change (ASLC) Rate using the Rates of TGSL and VLM

Date Period	TGSL Rate	VLM Rate from PSInSAR	Net ASLC Rate
December 2007 to December 2020	0.23 ± 0.63 mm/yr	-3.822 ± 0.713 mm/yr [a]	-3.592 ± 0.951 mm/yr

[a] The VLM Rate from PSInSAR was assumed to be constant

V. CONCLUSIONS AND RECOMMENDATIONS

The study was able to utilize tide gauge measurements, GNSS data, and InSAR technique (PSInSAR) to derive relative and net absolute sea level change at the tide gauge station in Mogpog, Marinduque. It also introduced an alternative method to determine local VLM near the tide gauge without a collocated GNSS receiver for the Philippines. The determination of the correlation of the PSInSAR LOS with LOS transformed GNSS displacements at the AGN station 6 km away from the tide gauge indicates the applicability of PSInSAR technique. The novelty of this research from the research conducted by CSLR-Phil is that it utilized a tide gauge without a collocated GNSS receiver as discussed previously, whereas the latter assessed sea level change in places where tide gauges have collocated GNSS receiver only.

The result of correlation between LOS from GNSS with LOS from PSInSAR at the AGN Station were 0.761 and 0.796 for ascending and descending, respectively. These indicate high correlation between the two datasets. Tide gauge measurements showed a near-zero sea level trend of 0.23 ± 0.63 mm/yr which is more positive than the computed absolute sea level change based on the technical report of CSLR-Phil [6]. This may indicate that the tide gauge station may have been experiencing subsidence. Looking at the results of PSInSAR, it confirms the hypothesis that the tide gauge experiences subsidence. After accounting for the VLM, the net absolute sea level change rate is -3.592 ± 0.951 mm/yr that indicates a downward trend. This result is consistent with the trend from other tide gauges with the same period of observation [6]. The reason for this trend was possibly due to the occurrence of El Nino between the observations in 2007 to 2019 that cause the sea level to fall. The estimated net absolute sea level change rate was not validated anymore since the VLM used to derive the said rate was already validated. PS points within 1 km of Station Balanacan exhibited large motion along LOS ascending geometry and may indicate movement along horizontal or vertical geometry or both. This has great implication on the stability of the said geodetic control.

The derived time series rate indicated that the AGN is moving at 10.785 mm/yr in N 58.57° W direction. Analysis of the data showed continuous linear movement with seasonal trend. There were no spikes in the time series which indicates that possibly, there were no occurrence of earthquakes with high magnitude during the period of observation.

The study showed the advantages of PSInSAR over GNSS stations as it can extract land motion on a much larger scale as compared to point-wise acquisition of GNSS stations. This study further proved that PSInSAR is important in sea level studies as it can give another perspective on the effects of increasing sea level. Moreover, the study can help policymakers in making decisions to reduce the effects of changing sea level and land subsidence.

The use of DEM with higher spatial resolution than the DEM used (SRTM 90m DEM) is recommended for further studies. Furthermore, study on sea level change projection in Mogpog, Marinduque can be explored to estimate future sea level change in the area and the possible risks that it may cause.

Due to the lack of PS points near Station Balanacan, and its location was not part of the coverage of the used descending images, establishment of cGNSS station may be necessary to

investigate its stability. Study of the local geology is also recommended for further studies to verify if the station is affected by factors such as soil composition, groundwater, and others. Densification of AGN stations can also benefit researchers studying, not only tectonic and volcanic activity, but also land subsidence and local sea level trends. More cGNSS stations can mean more validation points for studies utilizing satellite images quantifying land movement and sea level change.

REFERENCES

[1] Din AHM, Zulkifli NA, Hamden MH, Aris WAW. 2019. Sea level trend over Malaysian seas from multi-mission satellite altimetry and vertical land motion corrected tidal data. Advances in Space Research. 63(11):3452–3472. https://doi.org/10.1016/j.asr.2019.02.022

[2] Raucoules D, Le G, Wöppelmann G, de Michele M, Gravelle M, Daag A, Marcos M. 2013. Remote sensing of environment high nonlinear urban ground motion in Manila (Philippines) from 1993 to 2010 observed by DInSAR: Implications for sea-level measurement. Remote Sensing of Environment. *139*:386–397. https://doi.org/10.1016/j.rse.2013.08.021

[3] Philipppine Star (Cabico GK). 2019. Retrieved from https://www.philstar.com/headlines/2019/11/06/1966508/30-years-rising-seas-will-threaten-philippine-cities-towns-home-68m on Dec 2020.

[4] Mcleod E, Hinkel J, Vafeidis A, Nicholls R, Harvey N, Salm R. 2010. Sea-level rise vulnerability in the countries of the Coral Triangle. Sustainability Science. 5(2): 207-222. doi:10.1007/s11625-010-0105-1

[5] Mohamed B, Mohamed A, El-Din K, Nagy H. 2019. Sea level changes and vertical land motion from altimetry and tide gauges in the Southern Levantine Basin. Journal of Geodynamics. doi:10.1016/j.jog.2019.05.007

[6] [CSLR-Phil] Coastal Sea Level Rise - Philippines. 2021. Technical Report. Retrieved from sites.google.com/up.edu.ph/cslr-phil

[7] [CNES] National Centre for Space Studies. 2015. How Altimetry Works. CNES | Le site du Centre national d'études spatiales. Retrieved from https://cnes.fr/ on June 8, 2021.

[8] Avsar NB, Jin S, Kutoglu SH, Gurbuz G. 2017. Vertical land motion along the Black Sea coast from satellite altimetry, tide gauges and GPS. Advances in Space Research. 60(12):2871-2881. ScienceDirect. https://doi.org/10.1016/j.asr.2017.08.012

[9] Passaro M, Cipollini P, Vignudelli S, Quartly GD, Snaith HM. 2014. ALES: A multi-mission adaptive subwaveform retracker for coastal and open ocean altimetry. Remote Sensing of Environment. 145:173-189. ScienceDirect. http://dx.doi.org/10.1016/j.rse.2014.02.008

[10] Filmer MS, Williams SDP, Hughes CW, Wöppelmann G, Featherstone WE, Woodworth PL, Parker AL. 2020. An experiment to test satellite radar interferometry-observed geodetic ties to remotely monitor vertical land motion at tide gauges. Global and Planetary Change. 185(July 2019): 103084. https://doi.org/10.1016/j.gloplacha.2019.103084

[11] Belvis M, Taylor FW, Foster J. 2005. Sea level rise at Honolulu and Hilo, Hawaii: GPS estimates of differential land motion. Geophysical Research Letters. *32*. doi:10.1029/2004GL021380

[12] Bitharis S, Ampatzidis D, Pikridas C, Fotiou A, Rossikopoulos D, Schuh H. 2017. The role of GNSS vertical velocities to correct estimates of sea level rise from tide gauge measurements in Greece. Marine Geodesy. *40*(5): 297–314. https://doi.org/10.1080/01490419.2017.1322646

[13] Boretti A. 2020. Absolute and relative sea-level rise in the New York City area by measurements from tide gauges and satellite global positioning system. Journal of Ocean Engineering and Science. *xxxx*:1–8. https://doi.org/10.1016/j.joes.2020.05.001

[14] Caccamise DJ, Merrifield MA, Bevis M, Foster J, Firing YL, Schenewerk MS, Taylor FW, Thomas DA. 2005. Sea level rise at Honolulu and Hilo, Hawaii: GPS estimates of differential land motion. Geophysical Research Letters. *32*(3): 1–4. https://doi.org/10.1029/2004GL021380

[15] Parker A, Mörner N-A, Matlack-Klein P. 2018. Sea level acceleration caused by earthquake induced subsidence in the Samoa Islands. Ocean and Coastal Management. *161*:11-10. 10.1016/j.ocecoaman.2018.04.017

[16] Yang L, Francis OP. 2019. Sea-level rise and vertical land motion on the Islands of Oahu. Advances in Space Research. 2221-2232. doi:10.1016/j.asr.2019.08.028

[17] Montillet JP, Melbourne TI, Szeliga WM. 2018. GPS vertical land motion corrections to sea-level rise estimates in the Pacific Northwest. Journal of Geophysical Research: Oceans. 123(2), 1196–1212. https://doi.org/10.1002/2017JC013257

[18] Lu Y, Ke CQ, Zhou X, Wang M, Lin H, Chen D, Jiang H. 2018. Monitoring land deformation in Changzhou city (China) with multi-band InSAR data sets from 2006 to 2012. International Journal of Remote Sensing. 39(4):1151-1174. 10.1080/01431161.2017.1399474

[19] Crosetto M, Monserrat O, Cuevas-González M, Devanthéry N, Crippa B. 2016. Persistent scatterer interferometry: A review. ISPRS Journal of Photogrammetry and Remote Sensing. 78-89.

[20] Fuhrmann T, Garthwaite M. 2019. Resolving three-dimensional surface motion with InSAR: Constraints from multi-geometry data fusion. Remote Sensing.

[21] [PHIVOLCS] Philippine Institute of Volcanology and Seismology. Earthquake Information. 2018. Retrieved from dost.gov.ph on 2 Dec 2020.

[22] [ESA] European Space Agency. n.d.. Retrieved from https://sentinel.esa.int/web/sentinel/missions/sentinel-1/overview on 14 Dec 2020.

[23] Perissin D. 2021. SARPROZ (April 15, 2021) [PC Software]. https://www.sarproz.com

[24] [NOAA] National Oceanic and Atmospheric Administration. 2021. Retrieved from https://www.ncdc.noaa.gov/cdo-web on 15 Apr 2021

[25] Leys C, Ley C, Klein O, Bernard P, Licata L. 2013. Detecting outliers: Do not use standard deviation around the mean, use absolute deviation around the median. Journal of Experimental Social Psychology 49(4): 764-766

[26] Khorrami M, Abrishami S, Maghsoudi Y, Alizadeh B, Perissin D. 2020. Extreme subsidence in a populated city (Mashhad) detected by PSInSAR considering groundwater withdrawal and geothermal properties. Scientific Reports.

[27] Behera SK, Doi T, Luo J-J. 2021. Air–sea interaction in tropical Pacific: The dynamics of El Niño/Southern Oscillation. In Tropical and Extratropical Air-Sea Interactions. INC. https://doi.org/10.1016/b978-0-12-818156-0.00005-8

[28] Trenberth KE. 2019. El Niño southern oscillation (ENSO). In Encyclopedia of Ocean Sciences (3rd ed.). Elsevier Ltd. https://doi.org/10.1016/B978-0-12-409548-9.04082-3